THE GEOLOGICAL SOCIETY OF AMERICA®

Geochronological, geochemical, and Sr-Nd-Hf isotopic characteristics of granitoids in eastern Tibet and implications for tectonic correlation with southeastern Asia

Wang Shifeng*, Yao Xin, and Jiang Wan
INSTITUTE OF GEOMECHANICS, CHINESE ACADEMY OF GEOLOGICAL SCIENCES, BEIJING 100081, CHINA

ABSTRACT

Understanding the configuration of continental blocks within the Tibetan orogen prior to Indo-Asian collision is vital to determining their accretionary history. However, complex tectonic overprinting, including the development of the eastern and western Himalayan syntaxes, has hampered the investigation of correlations between tectonic blocks in the Tibetan Plateau with those in southeastern Asia. The North Lancangjiang tectonic belt is known to connect with the Longmu Co–Shuanghu suture to the west and the Changning-Menglian suture to the south, but limited work has been undertaken in eastern Tibet, and no ophiolite suites or high-pressure (HP) to ultrahigh-pressure (UHP) metamorphic belts have been identified within this belt. This paper presents new in situ zircon U-Pb, whole-rock major- and trace-element, and whole-rock Sr-Nd-Hf isotopic data for three granitic plutons (Chaya, Jinba, and Batang) within the North Qiangtang block. These plutons yield ages from ca. 265 Ma (Chaya) to ca. 230 Ma (Batang). The Chaya and Batang granites are chemically similar to I-type granites, whereas the Jinba granite is an S-type granite. Sr-Nd-Hf isotopic data suggest that the Chaya granite formed from magmas generated by the partial melting of subduction-modified mantle wedge material and that the Jinba granite formed from magmas generated by the partial melting of Precambrian metasedimentary rocks mixed with a small amount of juvenile mantle–derived crustal material. The Batang granite formed from magmas generated by the partial melting of mafic lower-crustal material. The convergence of the North Qiangtang block with neighboring blocks was a consequence of the closure of the Paleo-Tethys Ocean, and the plutons in this area record subduction-related or syncollisional magmatism. New data from granites within the North Lancangjiang magmatic belt and the Jinshajiang suture indicate that the North Lancangjiang Paleo-Tethyan slab subducted eastward, whereas the Jinshajiang Paleo-Tethyan slab subducted westward under the North Qiangtang block at ca. 267 Ma. The timing and style of block convergence between North Qiangtang–Simao–Indochina and neighboring blocks are similar to those recorded within central Tibet and southeastern Asia. This, combined with the presence of similar Middle Mesoproterozoic–Lower Paleozoic basement materials and Paleozoic sediments hosting Cathaysian warm-climate fossils, indicates that North Qiangtang, Simao, and Indochina represent a single block.

LITHOSPHERE GSA Data Repository Item 2019109 https://doi.org/10.1130/L1019.1

INTRODUCTION

The Himalayan-Tibetan orogen was formed by the sequential accretion of blocks onto the southern margin of Eurasia since the early Paleozoic. From north to south, these blocks include the Qaidam-Kunlun, Songpan-Ganzi (flysch belt), Qiangtang, Lhasa, and Himalayan blocks (Fig. 1A). The rifting and drifting of these blocks from Gondwana and their subsequent accretion onto Cathaysia are generally considered to have been related to the successive opening and closing of three intervening oceans, namely, the Paleo-Tethys (Devonian–Triassic), Meso-Tethys (late Early Permian–Late Cretaceous), and Neo-Tethys (Late Triassic–Late Cretaceous; Şengör, 1984; Metcalfe, 2013). Some blocks, such as the Cimmerian block (which includes the Turkey, Iran, Afghan, Qiangtang, Baoshan, and Sibumasu blocks), extend over a distance of >7000 km from the Mediterranean Sea in the west to the Sumatra arc in the east, whereas others (e.g., the Indochina, SW Borneo, and Simao blocks) are regarded as microcontinents, measuring 1000–2000 km long (e.g., Şengör, 1984; Metcalfe, 2013).

The correlation of the blocks that form the Tibetan Plateau with those in adjacent areas remains problematic as a result of the complex tectonic history of these amalgamated orogenic belts as well as subsequent widespread Cenozoic intracontinental deformation, particularly near the western and eastern Himalayan syntaxes (Fig. 1A). For example, the squeezing of the western syntaxis into the Pamir region during the Cenozoic has resulted in a debate over whether the southern or central Pamir should be regarded as the western continuation of the Qiangtang block, and whether the Shyok suture or Rushan-Pshart suture corresponds to the Bangong Co–Nujiang suture (Fig. 1A; e.g., Schwab et al., 2004; Angiolini et al., 2013). The relationships between blocks in southeastern Asia and those in Tibet are unclear, and many hypotheses have been proposed (e.g., Şengör, 1984; Royden et al., 2008; Pan et al., 2012; Metcalfe, 2013; Wang et al., 2016), including: (1) the Baoshan, Simao, and Shan Thai (Sibumasu) blocks represent the southeastern continuation of the Qiangtang block; (2) the Simao block represents an extension of the Qiangtang block, whereas the Baoshan and Shan Thai (Sibumasu) blocks correlate with the Lhasa block; (3) the Qiangtang block is divided into two parts, with the South Qiangtang block correlating with the Baoshan-Sibumasu block, and the

*Corresponding author: 948117360@qq.com; wsf@cags.ac.cn.

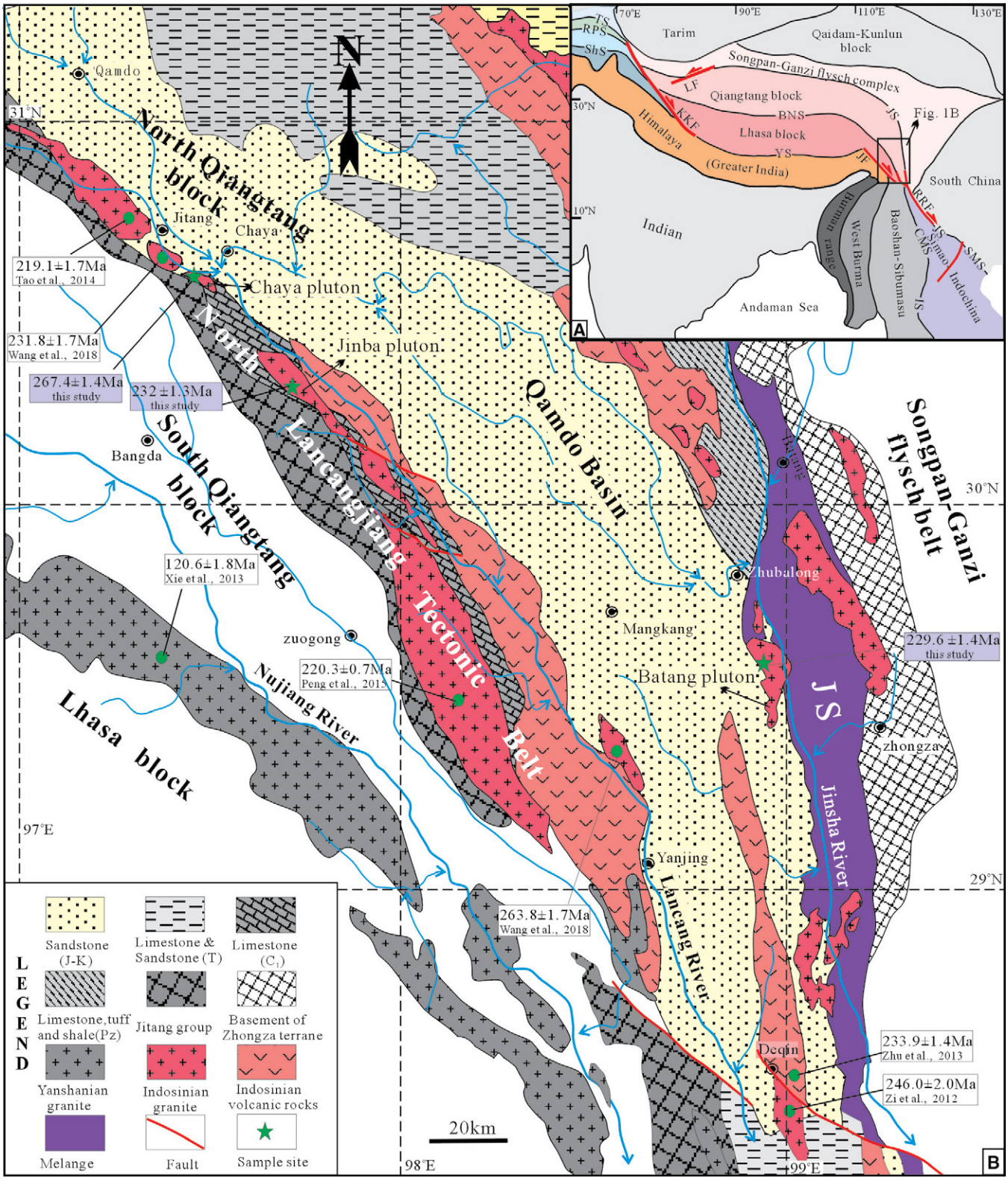

Figure 1. (A) Sketch map of the Tibetan Plateau and adjacent areas. (B) Geological map of the North Qiangtang block in the Qamdo area and the surrounding North Lancangjiang tectonic belt and Jinshajiang suture. Abbreviations are as follows: JS—Jinshajiang suture; BNS—Bangong Co–Nujiang suture; SMS—Song Ma suture; CMS—Changning-Menglian suture; IS—Inthanon suture; YS—Yalong-Zangpo suture; TS—Tanymas suture; RPS—Rushan–Pshart suture; ShS—Shyok suture; KKF—Karakorum fault; LF—Longmu Co fault; JF—Jiali fault; RRF—Red River fault. Time periods: J-K—Jurassic–Cretaceous; T—Triassic; C_1—Carboniferous; Pz—Paleozoic.

North Qiangtang block correlating with the Simao-Indochina block; and (4) blocks on the northern and southern sides of the eastern syntaxis are independent, or their relationships are unclear.

The limited research undertaken within the North Lancangjiang tectonic zone means that, to date, no ophiolitic or high-pressure (HP) to ultrahigh-pressure (UHP) rocks have been identified in this area. Recent research in this area has focused on the evolution of the Paleo-Tethyan system using petrological and geochemical data from Permian–Triassic granitoids within the North Lancangjiang magmatic belt (NLMB) section of the North Lancangjiang tectonic belt (e.g., Tao et al., 2014; Peng et al., 2015; Wang et al., 2018). However, more research is needed to further our understanding of the evolution of the Paleo-Tethys and the associated tectonic implications of this evolution. This study presents new zircon U-Pb and Lu-Hf isotopic, whole-rock major- and trace-element, and Sr-Nd isotopic data for the Permian–Triassic Chaya, Jinba, and Batang plutons of the Qamdo area of eastern Tibet. Combining these new data with the results of previous research enabled us to (1) determine the petrogenetic processes that controlled the formation of the granitoids, (2) constrain the timing and geometry of subduction of the North Lancangjiang and Jinshajiang Paleo-Tethyan slabs, and (3) provide insights into the correlation of blocks around the eastern Himalayan syntaxis.

GEOLOGIC SETTING IN THE QAMDO AREA

The basement of the Qamdo area in the North Qiangtang block is dominated by the Jitang Group, which contains biotite–plagioclase gneiss, biotite–hornblende gneiss, plagioclase amphibolite, and dark two-pyroxene granulite units (BGMRX, 1993). The protolith of the gneisses is dominantly a tuffaceous feldspar–quartz sandstone intercalated with volcanic rocks, argillaceous rocks, and carbonates. Mesozoic terrestrial clastics are widespread in the Qamdo area and have a thickness of several thousand meters. Paleozoic strata are restricted to the margins of the Qamdo basin and contain warm-water fossils (e.g., fusulinids, corals, and Gigantopterides; Li et al., 2009).

The North Lancangjiang tectonic belt separates the North and South Qiangtang blocks and connects to the Longmu Co–Shuanghu and Changning-Menglian suture zones; consequently, it is expected to contain relics of the Paleo-Tethys Ocean. However, the limited research undertaken in eastern Tibet means that no ophiolite suites or HP-UHP belts have been identified in this area to date. Late Permian–Triassic intermediate-felsic magmatic rocks crop out along the NLMB and connect with the Late Triassic volcanic rocks in central Qiangtang to the west (Fig. 1B), and with the Lincang batholith and Sukhothai arc to the south. Recent studies have attempted to reconstruct the evolution of the Paleo-Tethys using petrological and geochemical data from granitoids of the NLMB (Tao et al., 2014; Peng et al., 2015; Wang et al., 2018), but more reliable data are needed to constrain the different phases of block convergence.

The Jinshajiang-Ailaoshan tectonic belt, exposed along the eastern margin of the North Qiangtang block, is a suture zone that is thought to represent a branch of the Paleo-Tethys Ocean (Sun et al., 1997; Wang et al., 2000; Metcalfe, 2013). Ophiolitic mélange related to the closure of the Paleo-Tethys Ocean is observed along the entire Jinshajiang suture zone from southeastern Asia to the central Qiangtang area (Jian et al., 2009; Vuonga et al., 2013). A granitic magmatic belt is also widespread within the Jinshajiang suture zone and, in the Qamdo area, remains relatively unstudied.

Samples CY1-2, CY1-3, CY1-4, CY1-7, and CY1-8 were collected from the Chaya pluton, which was emplaced into Carboniferous limestones within the NLMB (Fig. 1B). The rocks are medium grained (average crystal sizes of 3–5 mm), are generally grayish white, and have little visible evidence of alteration or deformation. Optical microscopy indicates that these rocks are diorites consisting of 55–60 vol% plagioclase, 5 vol% quartz, 15 vol% biotite, and 20 vol% hornblende (Fig. 2A).

Samples JB-1 to JB-9 were collected from the Jinba pluton, which was emplaced into Carboniferous limestones and is unconformably covered by Triassic volcanic rocks within the NLMB (Fig. 1B). These grayish-white rocks are medium to coarse grained and have average crystal sizes of 4–8 mm. Optical microscopy indicates that these rocks are monzonitic granites consisting of 30 vol% plagioclase, 35 vol% K-feldspar, 25 vol% quartz, and 10 vol% biotite (Fig. 2B).

Samples BT-1 to BT-5 were collected from the Batang pluton, which was emplaced into the Jinshajiang ophiolitic mélange and is unconformably covered by Jurassic sandstones (Fig. 1B). The rocks are medium to coarse grained with average crystal sizes of 5–8 mm. Optical microscopy indicates that these rocks are monzonitic granites consisting of 35 vol% plagioclase, 30 vol% K-feldspar, 25 vol% quartz, 5 vol% biotite, and 5 vol% hornblende (Fig. 2C).

ANALYTICAL METHODS

Geochronological and geochemical data derived from granitic rocks can provide important information on the crustal evolution of tectonic plates. As such, six granite samples from two plutons within the NLMB and three further samples from one pluton in Jinshajiang suture belt were used for zircon U-Pb laser ablation–inductively coupled plasma–mass

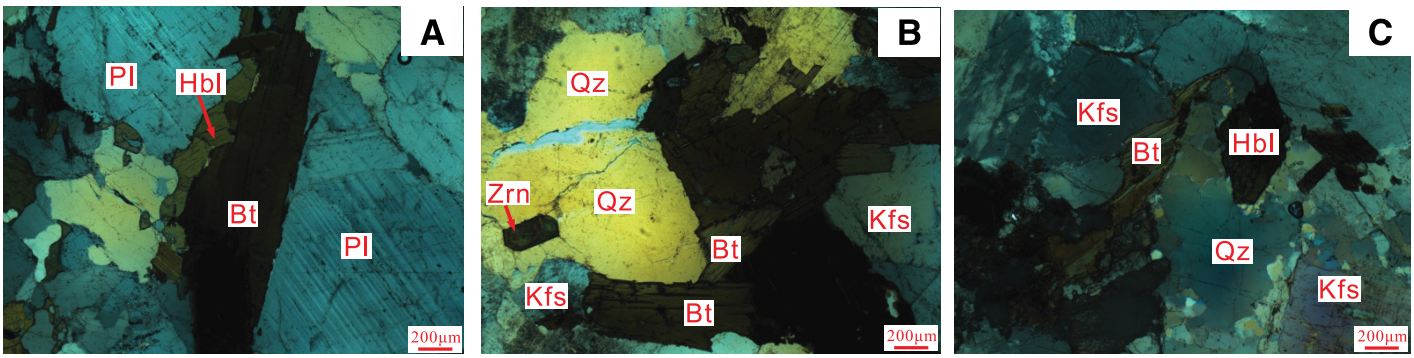

Figure 2. Photomicrographs of (A) diorite from the Chaya pluton and (B–C) monzonitic granites within the Jinba and Batang plutons. Abbreviations are as follows: Qz—quartz; Pl—plagioclase; Kfs—K-feldspar; Bt—biotite; Hbl—hornblende; Zrn—zircon.

spectrometry (LA-ICP-MS) dating during this study. Prior to analysis, zircons were separated using conventional heavy liquid and magnetic techniques. The resulting zircons were then purified by handpicking under a binocular microscope. Representative zircons were then mounted in epoxy resin before polishing to reveal zircon interiors prior to U-Pb dating. These zircons were examined and imaged both before and after analysis using transmitted and reflected light optical microscopy as well as cathodoluminescence (CL) to determine crystal shapes and internal structures and to pick positions for spot analyses.

Zircon U-Pb dating was undertaken using a New Wave UP193FX excimer LA system coupled with an Agilent 7500a ICP-MS instrument at the Key Laboratory of Continental Collision and Plateau Uplift, Institute of Tibetan Plateau Research, Chinese Academy of Sciences (CAS), Beijing, China. These analyses used a 36-μm-diameter laser beam and a 45 s ablation time. Helium was used as the carrier gas within the ablation cell to enhance the transport efficiency of the ablated materials. Raw count rates for ^{29}Si, ^{204}Pb, ^{206}Pb, ^{207}Pb, ^{208}Pb, ^{232}Th, and ^{238}U were collected for age determinations, with U, Th, and Pb concentrations as well as the concentrations of some other selected trace elements being calibrated using ^{29}Si as an internal standard and a NIST SRM 610 silicate glass standard as a reference material. The ^{207}Pb/^{206}Pb, ^{206}Pb/^{238}U, ^{207}Pb/^{235}U, and ^{208}Pb/^{232}Th isotopic ratios and age estimates were calculated using the Macquarie University GLITTER 4.0 program and were corrected using a 91500 zircon as an external standard. Weighted average age calculations and concordia diagram construction were undertaken using Isoplot/Ex version 3.0 (Ludwig, 2003). Age calculations were based on U decay constants of $^{235}U = 9.8454 \times 10^{-10}$ per annum and $^{238}U = 1.55125 \times 10^{-10}$ per annum (Ludwig, 2003), and common Pb corrections were made using the approach of Andersen (2002).

In situ zircon Lu-Hf isotopic analyses were conducted using a New Wave UP213 LA system coupled with a Neptune multicollector (MC) ICP-MS instrument at the State Key Laboratory for Mineral Deposits Research (SKLMDR), Nanjing University, Nanjing, China. The in situ zircon LA-ICP-MS Hf isotopic analyses used a beam size of 60 μm and a laser pulse frequency of 8 Hz. Details of the analytical approaches used and the methods used to correct for the interference of ^{176}Yb on ^{176}Hf are given in Wu et al. (2007). A ^{176}Lu decay constant of 1.865×10^{-11} per annum was used to calculate initial ^{176}Hf/^{177}Hf ratios, and the chondritic values of ^{176}Lu/^{177}Hf = 0.0332 and ^{176}Hf/^{177}Hf = 0.282772 reported by Blichert-Toft and Albarede (1997) were used to calculate $\varepsilon_{Hf}(t)$ values. Single-stage depleted mantle model ages (T_{DM1}) were calculated using a depleted mantle reservoir with a present-day ^{176}Hf/^{177}Hf value of 0.28325 and a ^{176}Lu/^{177}Hf value of 0.0384, whereas two-stage Hf model ages (T_{DM2}) were calculated using a ^{176}Lu/^{177}Hf value of 0.015 for the average continental crust (Griffin et al., 2000). A GJ-1 standard zircon was used for external standardization. The $\varepsilon_{Hf}(t)$ values were calculated using a decay constant of ^{176}Lu of 1.865×10^{-11} per annum, and all individual Hf isotopic analyses were located within previously ablated U-Pb analysis pits.

The whole-rock major- and trace-element compositions of 15 granite samples were determined during this study. Prior to analyses, these samples were powdered to <20 μm size using an agate mill. Major-element analyses were undertaken at the Institute of Geology and Geophysics, CAS, using a Phillips PW XFR-2400 X-ray fluorescence spectrometer, yielding an analytical uncertainty of <5% (±1σ). Trace-element concentrations, including those of the rare earth elements (REEs), were determined using solution ICP-MS at the Institute of Tibetan Plateau Research, CAS. Details of the operating conditions for the ICP-MS instrument and the data reduction approaches used have been given by Liu et al. (2008), with <5% uncertainties on all trace-element concentrations.

Whole-rock Rb-Sr and Sm-Nd isotopic analyses were undertaken using a Triton thermal ionization magnetic sector mass spectrometer at the School of Earth and Space Sciences, University of Science and Technology of China, Hefei, China, following the procedures outlined by Chen et al. (2007). Mass fractionation corrections for Sr and Nd isotopic ratios were based on ^{86}Sr/^{88}Sr = 0.1194 and ^{146}Nd/^{144}Nd = 0.7219.

NEW DATA FROM THE QAMDO AREA

In total, 19 samples from the three granitic plutons outlined above were selected for zircon U-Pb dating and in situ Hf isotopic analysis as well as whole-rock major- and trace-element analysis and Sr-Nd isotopic analysis. The resulting data are given in Tables DR1–DR4 in the GSA Data Repository Item[1] and are discussed below.

U-Pb Dating

Zircons extracted from three samples from the Chaya pluton commonly occur as light yellow to transparent, euhedral, prismatic grains. Cathodoluminescence (CL) images revealed luminescent cores, interpreted to reflect low U concentrations, and fine-scale euhedral oscillatory igneous zoning. The zircons typically range from 120 to 200 μm in length and 50–80 μm in width. Twenty-five representative zircons were selected from these samples for U-Pb dating (see Data Repository Table DR1). Th/U ratios showed ranges of 0.27–1.01, 0.32–1.11, and 0.27–0.97 for the three samples, respectively, indicating a magmatic origin. Results were tightly clustered and yielded weighted mean ^{206}Pb/^{238}U ages of 267.4 ± 1.4 Ma (CY1-2; mean square of weighted deviation [MSWD] = 0.78), 262 ± 1.3 Ma (CY1-3; MSWD = 0.27), and 260.9 ± 1.3 Ma (CY1-7; MSWD = 0.67; Figs. 3A–3C), which we interpret as the crystallization age of the Chaya granite.

Zircons from samples JB-2, JB-3, and JB-7 from the Jinba pluton occur as light yellow to transparent, euhedral prismatic grains. CL images revealed luminescent (low-U) cores and fine-scale euhedral oscillatory igneous zoning. The zircons typically range from 120 to 180 μm in length and 50–80 μm in width. Their characteristics are similar to those of zircon grains from the other plutons. We selected 25 representative zircons from the three samples for U-Pb dating (see Data Repository Table DR1). Th/U ratios showed ranges of 0.30–1.24, 0.24–0.75, and 0.13–1.08 for the three samples, respectively, indicating a magmatic origin. Results were tightly clustered and yielded weighted mean ^{206}Pb/^{238}U ages of 233.5 ± 1.3 Ma (JB-2; MSWD = 0.26), 232 ± 1.3 Ma (JB-3; MSWD = 0.74), and 232.2 ± 1.2 Ma (JB-7; MSWD = 0.64; Figs. 3D–3F), which we interpret as the crystallization age of the Jinba granitic complex.

Three samples from the Batang pluton were selected for U-Pb dating. CL images revealed luminescent (low-U) cores surrounded by fine-scale euhedral oscillatory igneous zoning. Th/U ratios showed ranges of 0.19–0.64, 0.19–0.36, and 0.10–0.52 for the three samples, respectively, indicating a magmatic origin. Results were tightly clustered and yielded weighted mean ^{206}Pb/^{238}U ages of 230.2 ± 1.2 Ma (BT-1; MSWD = 0.05), 229.8 ± 1.4 Ma (BT-2; MSWD = 0.11), and 229.6 ± 1.4 Ma (BT–3; MSWD = 0.25; Figs. 3G–3I), which we interpret as the crystallization age of the Batang granitic complex.

[1]GSA Data Repository Item 2019109, Table DR1: LA-ICP-MS U-Pb analyses of zircon grains from the Chaya, Jinba, and Batang plutons in eastern Tibet; Table DR2: Lu-Hf isotopic compositions of zircons from the Chaya, Jinba, and Batang plutons; Table DR3: Major-element (wt%) and trace element (ppm) concentrations of the Chaya, Jinba, and Batang plutons; Table DR4: Sr-Nd isotopic compositions of selected samples from the Chaya, Jinba, and Batang plutons, is available at http://www.geosociety.org/datarepository/2019, or on request from editing@geosociety.org.

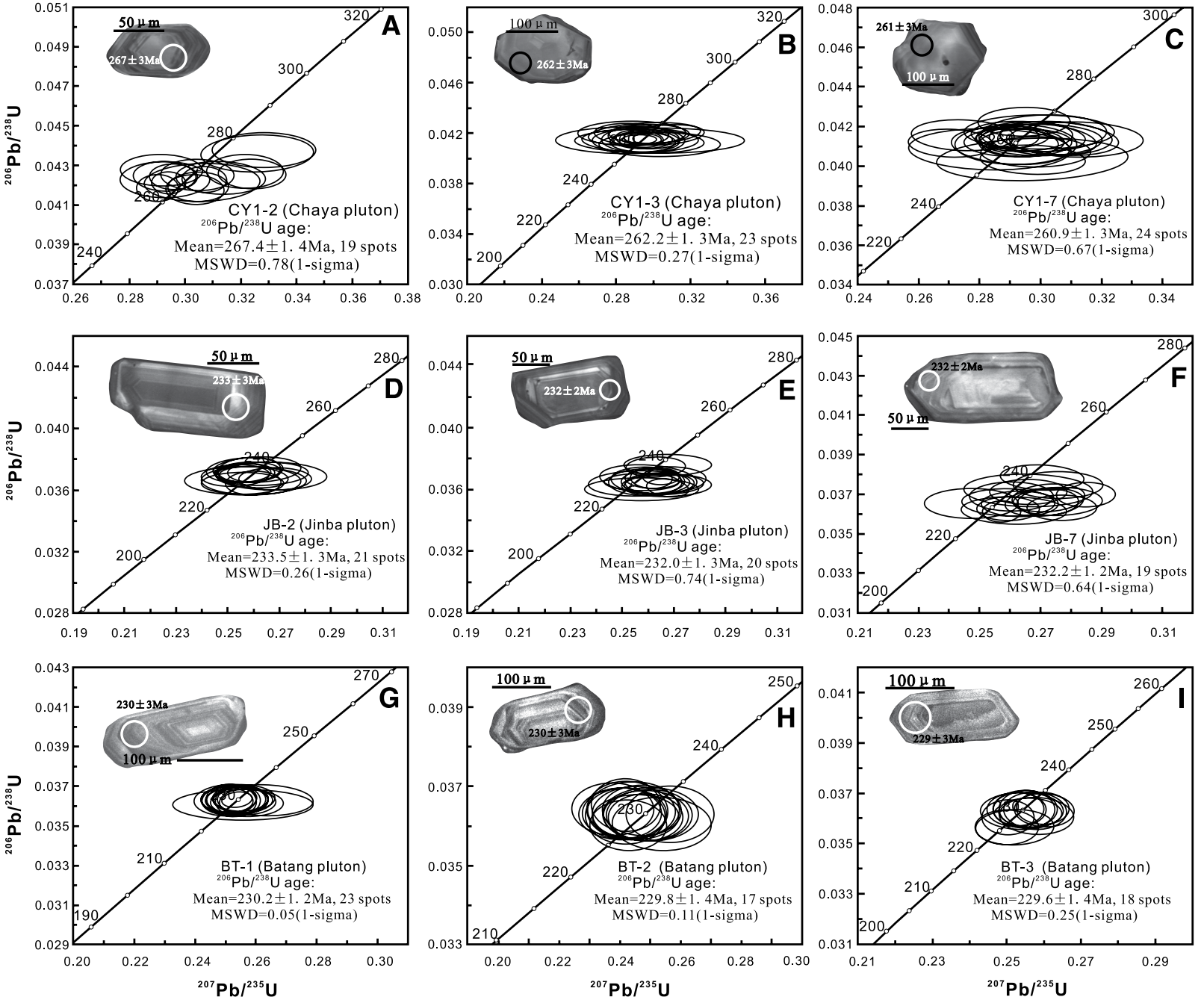

Figure 3. Cathodoluminescence (CL) images of representative zircon grains from the granitic plutons in the North Lancangjiang magmatic belt and the Jinshajiang suture, with corresponding concordia diagrams. MSWD—mean square of weighted deviates.

Zircon Lu-Hf Isotopic Analysis

We selected eight samples (CY1-2, CY1-3, CY1-7, JB-2, JB-3, JB-7, BT-1, and BT-2) for in situ Lu-Hf isotopic analysis and analyzed ~15 spots in each sample. The results are listed in Data Repository Table DR2 and are shown in Figure 4.

Forty-five analyses of zircon grains from the Chaya pluton yielded initial $^{176}Hf/^{177}Hf$ ratios of 0.282766–0.282887 and $\varepsilon_{Hf}(t)$ values of +4.79 to +10.58. Corresponding Hf crustal two-stage model ages (T_{DM2}) ranged from 928 to 718 Ma, with a mean of 804.7 Ma.

Forty-five analyses of zircon grains from the Jinba pluton yielded initial $^{176}Hf/^{177}Hf$ ratios of 0.282597–0.282810 and $\varepsilon_{Hf}(t)$ values of –1.04 to +6.46. Corresponding Hf crustal T_{DM2} ages ranged from 1327 to 896 Ma, with a mean of 1018.7 Ma.

Thirty analyses of zircon grains from the Batang pluton yielded initial $^{176}Hf/^{177}Hf$ ratios of 0.282064–0.282441 and $\varepsilon_{Hf}(t)$ values of –20.17 to –7.04. Hf crustal T_{DM2} ages ranged from 2526 to 1691 Ma, with a mean of 1828.1 Ma.

Whole-Rock Major-Element, Trace-Element, and REE Analyses

Nineteen samples were selected from the three plutons for major-element, trace-element, and REE analyses (see Data Repository Table DR3). As seen in the ($Na_2O + K_2O$) versus SiO_2 diagram (Fig. 5A), samples from the Chaya pluton are typically classified as diorites, whereas Jinba and Batang samples lie within the granite field.

Chaya Pluton

Five representative samples of the Chaya pluton were selected for whole-rock major- and trace-element analyses (see Data Repository Table DR3). The diorite samples are compositionally homogeneous, with SiO_2 = 58.10–62.97 wt%, total alkalis ($K_2O + Na_2O$) = 5.42–6.29 wt%, CaO = 4.01–6.21 wt%, Al_2O_3 = 16.28–18.16 wt%, MgO = 1.58–3.22 wt%, Fe_2O_3 = 5.53–7.75 wt%, and TiO_2 = 0.92–1.36 wt%. On a K_2O versus Si_2O classification diagram, the samples plot in the low-K calc-alkaline field (Fig. 5B). A/CNK values (molar $Al_2O_3/[CaO + K_2O + Na_2O]$) range from 0.85 to 0.97 (see Data Repository Table DR3), which are typical of metaluminous I-type granitoids (Fig. 5C). Samples from the Chaya pluton show relatively high Mg# (36.14–45.91), higher than those predicted for purely crust-derived partial melts. In addition, all of these samples plot in the I- and S-type granite field of a Y versus Ga/Al diagram, with none plotting in the A-type granite field.

Chondrite-normalized REE and primitive-mantle–normalized trace-element concentrations for the Chaya diorites are shown in Figures 6A–6B. The Chaya diorites are enriched in large ion lithophile elements (LILEs; e.g., Rb, U, and Th) and depleted in high field strength elements (HFSEs; e.g., Ta, Nb, P, and Ti). They have high light REE (LREE) concentrations (132–212 ppm) and relatively low heavy REE (HREE) concentrations (13–22 ppm), yielding LREE/HREE ratios of 6.5–10.6. The samples display weakly negative to positive Eu anomalies, with Eu/Eu* values of 0.87–1.07. In the Rb (ppm) versus (Yb + Ta) (ppm) tectonic classification diagram (Pearce and Peate, 1995), all granitic samples from the Chaya pluton plot within the volcanic arc granite (VAG) field (Fig. 5F).

Jinba Pluton

Nine representative samples of the Jinba pluton were selected for whole-rock major- and trace-element analyses (see Data Repository Table DR3). The granitic samples are classified as high-Si granites, with SiO_2 = 70.96–74.08 wt%, total alkalis = 8.41–9.04 wt%, CaO = 0.29–1.32 wt%, Al_2O_3 = 12.95–14.37 wt%, MgO = 0.22–0.73 wt%, Fe_2O_3 = 1.61–2.67 wt%, and TiO_2 = 0.16–0.25 wt%. On a K_2O versus Si_2O classification diagram, the samples plot in the high-K calc-alkaline to shoshonite fields

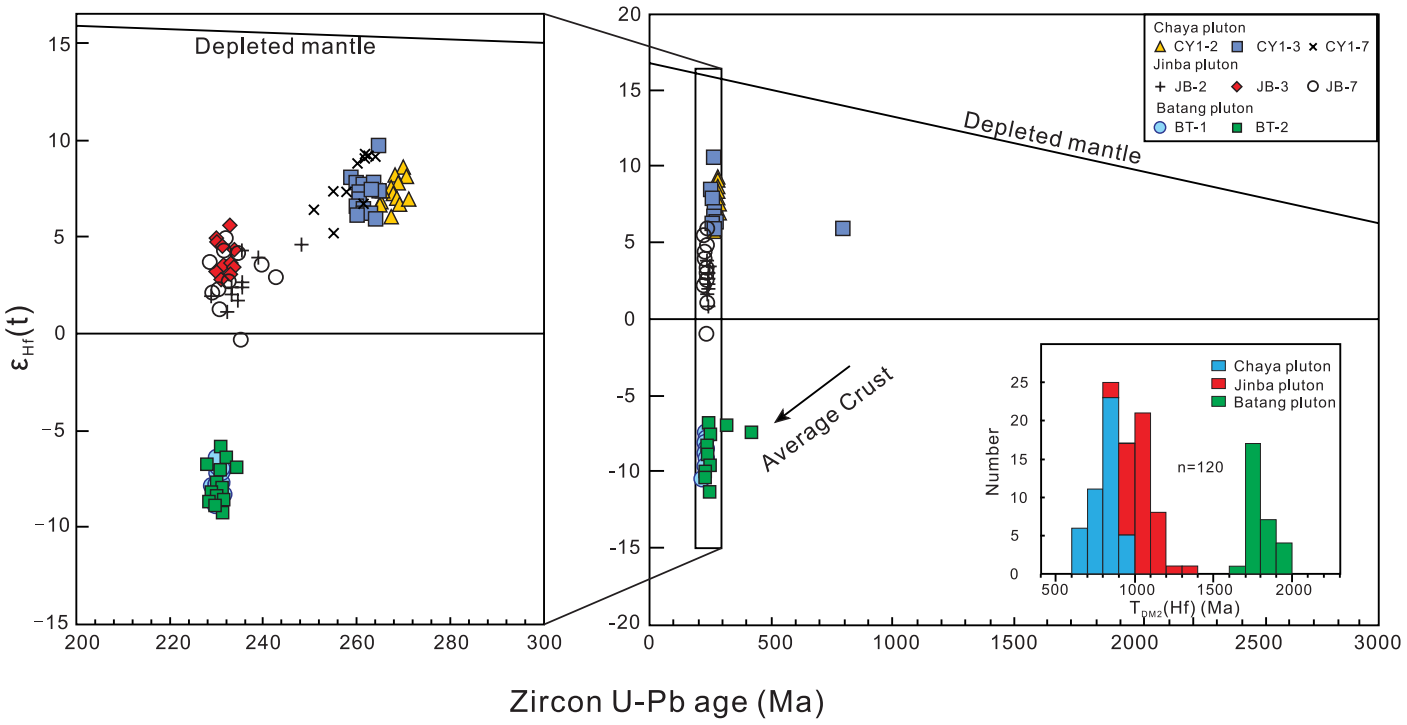

Figure 4. $\varepsilon_{Hf}(t)$ vs. U-Pb ages for granites of the Chaya, Jinba, and Batang plutons. Hf isotopic compositions of chondrite and depleted mantle are from Blichert-Toft and Albarede (1997).

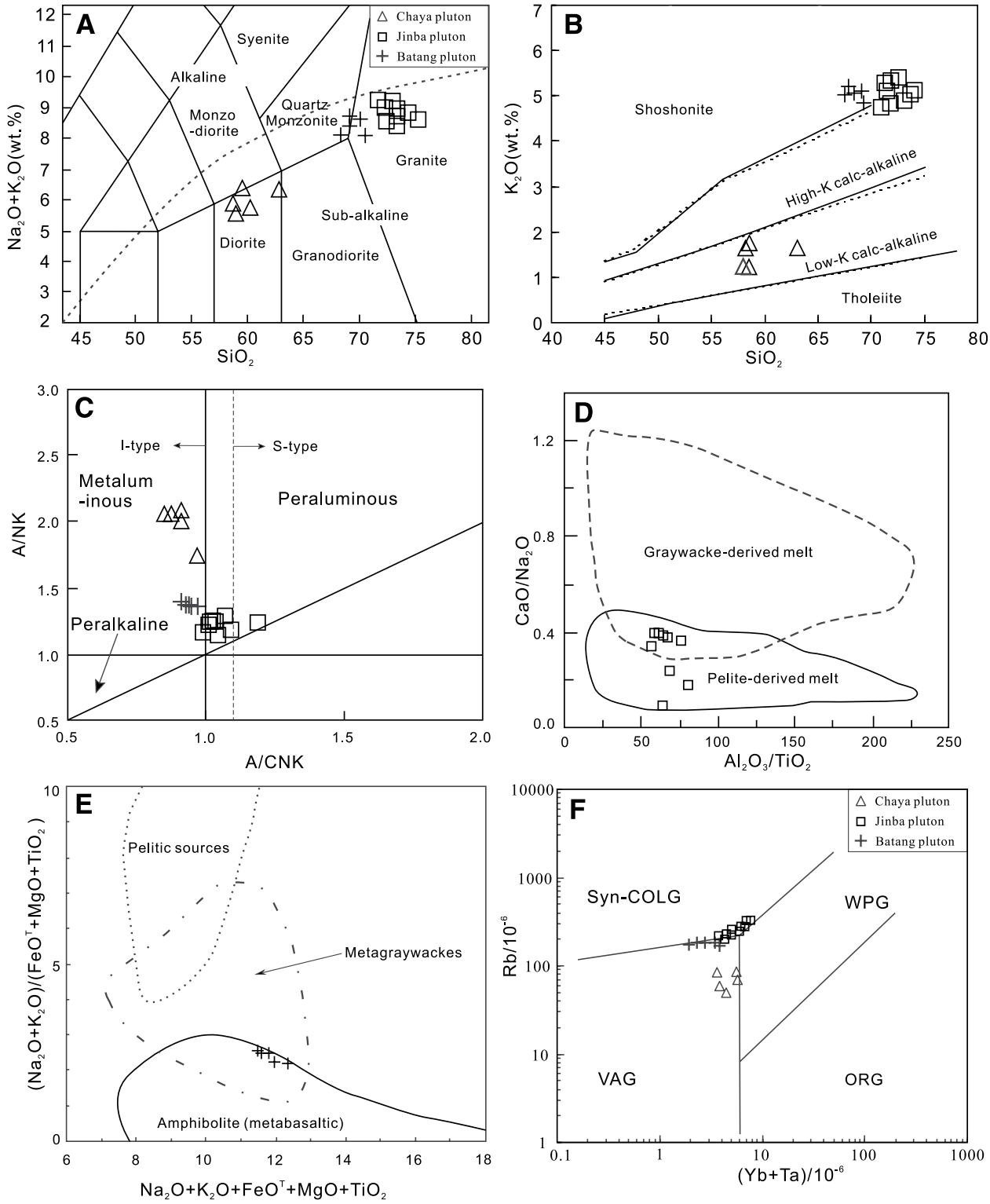

Figure 5. Diagrams showing the geochemical compositions of the Chaya, Jinba, and Batang granitoids. (A) ($K_2O + Na_2O$) vs. SiO_2 diagram (after Middlemost, 1994) showing the classification of the Chaya, Jinba, and Batang granitoids; (B) K_2O vs. SiO_2 diagram (after Peccerillo and Taylor, 1976) illustrating the calc-alkaline to high-K calc-alkaline nature of the Chaya, Jinba, and Batang samples; (C) A/CNK (molar $Al_2O_3/[CaO + Na_2O + K_2O]$) vs. A/NK (molar $Al_2O_3/[Na_2O + K_2O]$) diagram (after Maniar and Piccoli, 1989) indicating the I- and S-type nature of the Chaya, Jinba, and Batang granites; (D) CaO/Na_2O vs. Al_2O_3/TiO_2 (after Jung and Pfänder, 2007); (E) $(Na_2O + K_2O)/(FeO_T + MgO + TiO_2)$ vs. $Na_2O + K_2O + FeO_T + MgO + TiO_2$ (in wt%; after Patiño Douce, 1999) diagrams indicating magma source characteristics for the Jinba and Batang plutons; and (F) $Rb/10^{-6}$ vs. $(Yb + Ta)/10^{-6}$ discrimination diagrams (after Pearce and Peate, 1995) used to identify the tectonic settings of the Chaya, Jinba, and Batang plutons. VAG—volcanic arc granite; ORG—oceanic ridge granite; WPG—within-plate granite; Syn-COLG—syncollision granite.

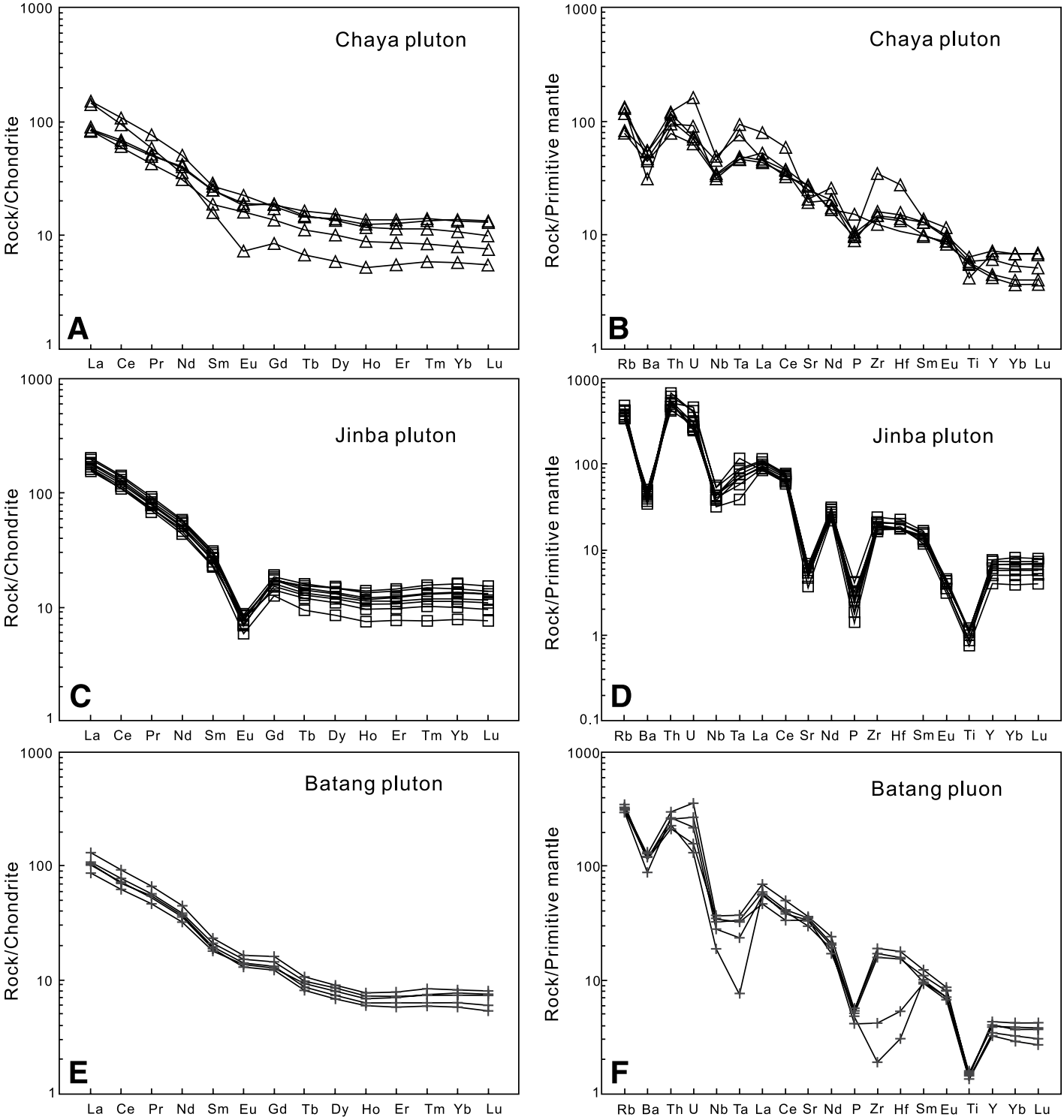

Figure 6. Chondrite-normalized rare earth element (REE) and primitive-mantle–normalized trace-element concentrations of the Chaya (A–B), Jinba (C–D), and Batang (E–F) granitoids. Chondrite and primitive mantle compositions are from Boynton (1984) and Sun and McDonough (1989), respectively.

(Fig. 5B). A/CNK values range from 0.98 to 1.18 (see Data Repository Table DR3), which are typical of peraluminous S-type granitoids (Fig. 5C). In addition, all of these samples plot in the I- and S-type granite field of a Y versus Ga/Al diagram, with none plotting in the A-type granite field.

Chondrite-normalized REE and primitive-mantle–normalized trace-element concentrations for the Jinba granites are shown in Figures 6C–6D. The Jinba granites are enriched in LILEs and depleted in HFSEs. They have high LREE concentrations (212–273 ppm) and relatively low HREE concentrations (13–22 ppm), yielding LREE/HREE ratios of 10.0–16.8. The samples display pronounced negative Eu anomalies, with Eu/Eu* values of 0.34–0.45. In the Rb (ppm) versus (Yb + Ta) (ppm) tectonic classification diagram, all of the granitic samples plot within the syncollision field (Fig. 5F).

Batang Pluton

Five representative samples of the Batang pluton were selected for whole-rock major- and trace-element analyses (see Data Repository Table DR3). The granitic samples contain 67.83–69.20 wt% SiO_2, 8.22–8.57 wt% total alkalis, 2.42–2.95 wt% CaO, 14.71–15.15 wt% Al_2O_3, 0.77–1.04 wt% MgO, 2.39–2.74 wt% Fe_2O_3, and 0.29–0.32 wt% TiO_2. On a K_2O versus Si_2O classification diagram, the samples plot in the shoshonite field (Fig. 5B). A/CNK values range from 0.92 to 0.97 (Data Repository Table DR3), which is typical of metaluminous I-type granitoids (Fig. 5C). In addition, all of these samples plot in the I- and S-type granite field of a Y versus Ga/Al diagram, with none plotting in the A-type granite field.

Chondrite-normalized REE and primitive-mantle–normalized trace-element patterns for the Batang granites are shown in Figures 6E–6F. The Batang granites are enriched in LILEs and depleted in HFSEs. They have high LREE concentrations (126–185 ppm) and relatively low HREE concentrations (11–14 ppm), yielding LREE/HREE ratios of 10.0–13.9. The samples display weakly negative Eu anomalies, with Eu/Eu* values of 0.84–0.89. On the Rb (ppm) versus (Yb + Ta) (ppm) tectonic classification diagram, all granitic samples plot along the boundary between the syncollision and arc magmatic fields (Fig. 5F).

Sr-Nd Isotopic Compositions

Sr and Nd isotopic compositions of the Chaya, Jinba, and Batang plutons are given in Data Repository Table DR4.

Chaya Pluton

Three Chaya diorite samples were selected for Sr-Nd isotopic analysis. They exhibit low $^{87}Sr/^{86}Sr$ (0.707089–0.707704) and high $^{143}Nd/^{144}Nd$ ratios (0.512581–0.512910; see Data Repository Table DR4). Initial $^{87}Sr/^{86}Sr$ ratios vary from 0.705524 to 0.706048, and $\varepsilon_{Nd}(t)$ values range from +1.69 to +7.71. The samples yield T_{DM2}(Nd) model ages of 892–406 Ma (Data Repository Table DR4).

Jinba Pluton

Three samples of the Jinba pluton were selected for Sr-Nd isotopic analysis. They exhibit high $^{87}Sr/^{86}Sr$ ratios (0.726963–0.734123) and a narrow range of $^{143}Nd/^{144}Nd$ ratios (0.512354–0.512359; see Data Repository Table DR4). Initial $^{87}Sr/^{86}Sr$ ratios vary from 0.706301 to 0.706969, and $\varepsilon_{Nd}(t)$ values range from –2.78 to –2.59. The samples yield a narrow range of T_{DM2}(Nd) model ages of 1232–1217 Ma (Data Repository Table DR4).

Batang Pluton

Three samples of the Batang pluton were selected for Sr-Nd isotopic analysis. They exhibit low $^{87}Sr/^{86}Sr$ (0.712251–0.712434) and $^{143}Nd/^{144}Nd$ (0.512026–0.512351) ratios (Data Repository Table DR4). Initial $^{87}Sr/^{86}Sr$ ratios vary from 0.709367 to 0.709725, and $\varepsilon_{Nd}(t)$ values range from –9.17 to –2.78. The samples yield T_{DM2}(Nd) model ages of 1748–1230 Ma (see Data Repository Table DR4).

DISCUSSION

Origin of the Plutons

Here, we used our acquired geochemical data to infer details regarding the origin of plutons in the Qamdo area and assess their role in the evolution of the Paleo-Tethys Ocean.

Origin of the Chaya Pluton

Chaya pluton samples contain amphibole (Fig. 2A) and 58.1–62.9 wt% SiO_2, yielding low A/CNK values (0.85–0.98; mean = 0.91) and weakly negative to positive Eu anomalies (Eu/Eu* = 0.87–1.04), indicating that they represent metaluminous, I-type granitoids (Fig. 5C). They also exhibit high LILE/HFSE ratios, pronounced negative Nb, Ta, P, and Ti anomalies, and positive $\varepsilon_{Nd}(t)$ values (+1.69 to +7.71), features characteristic of arc magmas.

The formation of arc magmas is generally attributed to partial melting of the underlying mantle wedge or underplated mafic lower crust (Pearce and Peate, 1995). As the Chaya pluton samples yield positive $\varepsilon_{Nd}(t)$ values (+1.69 to +7.71) and positive $\varepsilon_{Hf}(t)$ values (+4.79 to +10.58), it is unlikely that the pluton was produced by the partial melting of underplated mafic lower crust, which typically results in negative $\varepsilon_{Nd}(t)$ values. We therefore infer that the Chaya pluton was generated by partial melting of the underlying mantle wedge.

The radiogenic Sr and Nd isotopic compositions of the Chaya pluton granitoids (Fig. 7A) were likely inherited from a mantle source that was previously metasomatized by slab-derived melts/fluids. In general, metasomatism related to fluids/melts released from subducting oceanic slabs does not affect the Nd composition of overlying mantle, which typically yields homogeneous $\varepsilon_{Nd}(t)$ values (Gertisser and Keller, 2003), in contrast to the highly variable Nd compositions of samples from the Chaya pluton. Therefore, we infer that the highly variable Nd compositions of the Chaya pluton resulted from modification of the upper mantle by subducted sediments (and/or melts derived thereof), rather than metasomatism by fluids/melts released from a subducting slab. This hypothesis is supported by the high Al_2O_3 concentrations (16.28–18.16 wt%) and low Ce/Pb ratios (0.4–1.7) in Chaya pluton samples, which also suggest the involvement of subducted sedimentary materials in the source region (Murphy et al., 2018). The positive ε_{Nd} and ε_{Hf} values of the Chaya samples mean that these samples generally plot in the mid-ocean-ridge basalt (MORB) field of a $\varepsilon_{Nd}(t)$ versus $\varepsilon_{Hf}(t)$ diagram (Fig. 7B), supporting a mantle source for these granites. Zircon saturation temperatures for the Chaya granitoids range from 749 °C to 843 °C (average of 765 °C; Data Repository Table DR3; Watson and Harrison, 1983), indicating that the Chaya granitoids are low-temperature granitoids (Miller et al., 2003). Low-temperature granitoids are thought to form as a result of the addition of subducted fluids released from subducted sedimentary material to the mantle. This suggests that the source of the low-temperature Chaya granitoids contained subducted sedimentary material.

Origin of the Jinba Pluton

Granites from the Jinba pluton exhibit high SiO_2 concentrations (71.0–74.1 wt%) and A/CNK values (0.98–1.18; mean = 1.04), have pronounced negative Eu anomalies, and contain no metaluminous minerals (e.g., hornblende or titanite; Fig. 2B), suggesting that they represent peraluminous S-type granites. Geochemical and isotopic data and constraints

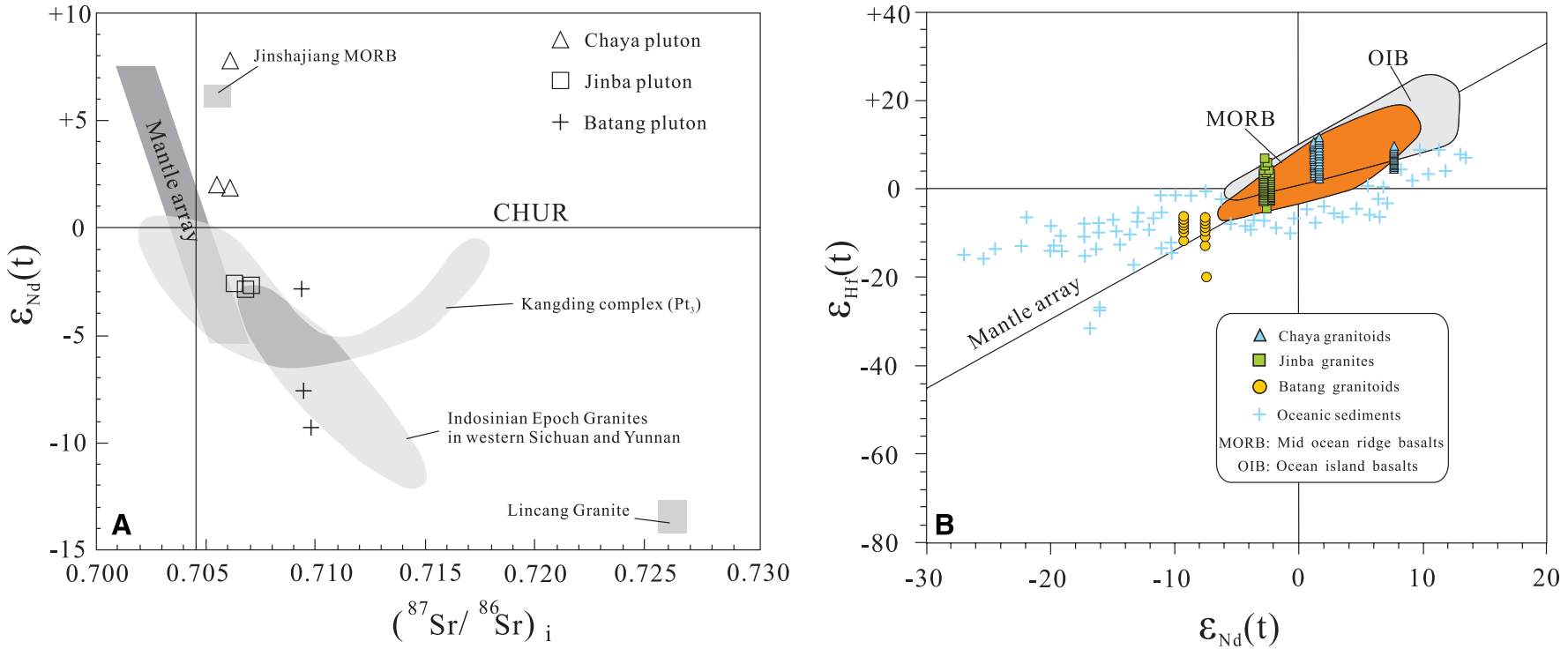

Figure 7. Diagrams showing variations in the isotopic compositions of the granites in the study area: (A) $\varepsilon_{Nd}(t)$ vs. initial $^{87}Sr/^{86}Sr$, and (B) $\varepsilon_{Hf}(t)$ vs. $\varepsilon_{Nd}(t)$. Oceanic sediment compositions are from Zhang et al. (2012). CHUR—chondritic uniform reservoir; Pt_3—Neo-Proterozoic.

from petrological experiments suggest that large-volume peraluminous granites are typically produced during the melting of crustal rocks (e.g., Petford and Atherton, 1996; Patiño Douce, 1999; Clemens, 2003) from diverse protoliths, which include: (1) aluminum-rich metasediments such as metapelites and graywackes; (2) quartzofeldspathic meta-igneous rocks such as orthogneiss; and (3) basic meta-igneous rocks such as amphibolites. Experimental studies have shown that magmas derived from the partial melting of basic meta-igneous rocks (amphibolites) have high Na values, low HREE contents, and high Al compositions, preserve evidence of residual garnet, clinopyroxene, and amphibole (Petford and Atherton, 1996), and are strongly depleted in LILEs, U, and Th (Clemens, 2003). The Jinba granites, however, lack such signatures (Data Repository Table DR3; Fig. 3D). In addition, their initial $^{87}Sr/^{86}Sr$ values and low $\varepsilon_{Nd}(t)$ values (Data Repository Table DR4) are inconsistent with those of the basement in the North Qiangtang block (Tao et al., 2014). We therefore exclude the possibility that the Jinba granites were derived from lower-crustal meta-igneous rocks.

In general, granites derived from orthogneiss or psammite sources exhibit high CaO/Na_2O and low Al_2O_3/TiO_2 ratios (Clemens, 2003), in contrast to the low CaO/Na_2O (0.08–0.36) and high Al_2O_3/TiO_2 (57.4–80.9) ratios of the Jinba pluton samples. We therefore infer that metapelites were the most likely source for the Jinba granites. This inference is supported by the CaO/Na_2O versus Al_2O_3/TiO_2 diagram, in which most samples plot within the pelite source field (Fig. 5D). We propose that such a source corresponds to metasedimentary rocks of the Precambrian Jitang Group in North Qiangtang, which include meta-graywacke, metapelite, and minor interlayered meta-basalt. However, the Jitang Group yields negative $\varepsilon_{Nd}(t)$ values that are lower than those of the Jinba granites. We interpret this discrepancy to be the result of the interaction between mantle-derived juvenile crust (high $\varepsilon_{Nd}[t]$) and the metapelitic source.

The Kangding pluton, located on the western margin of the Yangtze block, is considered to represent the basement of the Yangtze craton (Xu et al., 2004). In a $(^{87}Sr/^{86}Sr)_i$ versus $\varepsilon_{Nd}(t)$ diagram (Fig. 7A), all of the Jinba pluton samples from the North Qiangtang block plot within the field representing the composition of the Kangding pluton. Consequently, we suggest that the North Qiangtang block has an affinity with the Yangtze block. This is consistent with the drifting of the Qamdo-Simao block from the Yangtze block during the early Paleozoic before accreting to the latter between the Late Permian and Early Triassic (Sun et al., 1997; Wang et al., 2000; Jian et al., 2009; Yang et al., 2011).

The negative ε_{Nd} and positive ε_{Hf} values for the Jinba granites plot in the MORB and oceanic-island basalt (OIB) fields of a $\varepsilon_{Nd}(t)$ versus $\varepsilon_{Hf}(t)$ diagram (Fig. 7B), indicating that the formation of these granites involved the upwelling of asthenospheric material beneath their source region within the lower continental crust. Zircon saturation temperatures for the Jinba granitoids range from 794 °C to 833 °C (average of 810 °C; Data Repository Table DR3; Watson and Harrison, 1983), indicating that these granites are high-temperature granitoids (Miller et al., 2003). High-temperature granitoids are thought to be associated with the upwelling of asthenospheric material, supporting a model in which the high-temperature Jinba granitoids formed as a result of asthenospheric upwelling beneath their magma source region.

Origin of the Batang Pluton

Granites from the Batang pluton contain 67.83–69.20 wt% SiO_2, exhibit low A/CNK values (0.92–0.97), have weakly negative Eu anomalies (Eu/Eu* = 0.84–0.89), and contain metaluminous minerals (hornblende; Fig. 2C), suggesting an I-type affinity. Previous studies have suggested that I-type granitoids are generated through partial melting of intracrustal metamorphosed mafic to intermediate igneous rocks (Chappell and White, 1992). Melting of intermediate igneous rocks, such as quartz diorites, typically yields highly peraluminous melts (Patiño Douce, 1999), in contrast to the metaluminous granites of the Batang pluton. The melting of metabasaltic sources at high temperatures is capable of producing metaluminous melts (Rapp et al., 1991); however, low-K_2O basaltic source rocks are an unsuitable source for the high-K_2O Batang granites (Fig. 5B). Melts derived from basaltic amphibolites are similar to the high-K calc-alkaline Batang granites (Patiño Douce, 1999). In a $(Na_2O + K_2O + FeO^T + MgO + TiO_2)$ versus $(Na_2O + K_2O)/(FeO^T + MgO + TiO_2)$ magma source discrimination diagram (Fig. 5E), most samples plot within the metabasaltic amphibolite field, further supporting a model in which the Batang granites were derived from a metabasaltic source within the lower crust. This is also supported by the negative ε_{Nd} and ε_{Hf} values for the Batang granites, which plot in the oceanic crustal field of a $\varepsilon_{Nd}(t)$ versus $\varepsilon_{Hf}(t)$ diagram (Fig. 7B). In addition, the Batang granites have whole-rock zircon saturation temperatures that range from 625 °C to 792 °C (average of 733 °C; Data Repository Table DR3; Watson and Harrison, 1983), indicating that they are low-temperature granitoids (Miller et al., 2003) most likely derived from the in situ melting of a lower-crustal source.

The Batang granites display variable Sr and Nd isotopic compositions (Data Repository Table DR4), indicating crustal contamination of the magma that formed the Batang pluton. In a $(^{87}Sr/^{86}Sr)_i$ versus $\varepsilon_{Nd}(t)$ diagram, samples from the Batang pluton (located on the eastern margin of the North Qiangtang block) plot close to the field of Kangding pluton compositions, further supporting our inference that the North Qiangtang block has an affinity with the Yangtze block. In addition, Indosinian granitoids from western Sichuan and Yunnan Provinces have Sr and Nd isotopic compositions that are similar to those of the Batang pluton (Fig. 7A) and may therefore have been derived from a similar source. However, more data are required to confirm this correlation.

Timing and Style of Convergence between the North Qiangtang and Adjacent Blocks

Closure of the North Lancangjiang Paleo-Tethys Ocean

Several studies have investigated the geochronology and petrogenesis of the intermediate-felsic magmatic rocks of the NLMB (Tao et al., 2014; Peng et al., 2015; Wang et al., 2018). Igneous zircons from five quartz diorite samples from the Xiaochangdu pluton yielded weighted mean U-Pb ages of ca. 263–257 Ma. In addition, three granitic and two dioritic samples from the intermediate-felsic Kagong pluton yielded coeval ages between 234 and 232 Ma (Wang et al., 2018). These two plutons record the two stages of convergence of the North and South Qiangtang blocks along the north Lancangjiang tectonic belt (Wang et al., 2018). These ages are older than those obtained from the Jitang pluton (ca. 220 Ma), which is interpreted to have formed during postcollisional magmatism following the closure of the Paleo-Tethys Ocean (Tao et al., 2014). The 267–232 Ma zircon ages for the Chaya and Jinba granites of the NLMB obtained during this study are similar to the emplacement ages obtained for the Xiaochangdu, Kagong, Jitang, and Dongdashan plutons within the NLMB (Fig. 1B), suggesting that all of these plutons record the same period of Paleo-Tethyan evolution. The NLMB also contains an ~300-km-long ductile shear zone (BGMRX, 1993) that has a stable geometry indicative of the northeastward-directed thrusting of the South Qiangtang block under the North Qiangtang block.

The NLMB in the Qamdo area connects with the Late Permian to Early Triassic magmatic rocks in central Qiangtang to the west (e.g., Zhang et al., 2006; Zhai et al., 2016) and with the Lincang batholith and Sukhothai arc to the southeast (e.g., Peng et al., 2008; Gardiner et al., 2016) to form one continuous Indosinian magmatic belt. Whole-rock major-element,

trace-element, and REE data from the Chaya pluton are comparable with those reported from I-type arc granites. The Chaya pluton has 267–260 Ma subduction-related I-type granites that are similar to those in the Sukhothai belt, adjacent to the Inthanon suture zone (Gardiner et al., 2016). In contrast, the 233.5–232 Ma Jinba pluton contains syncollisional granites, similar to those commonly observed in the Lincang-Sukhothai belt (e.g., Peng et al., 2008; Tao et al., 2014; Gardiner et al., 2016). We suggest that convergence between the North and South Qiangtang blocks can be divided into two stages occurring at 267–233.5 and 233.5–200 Ma. The first stage represents the eastward subduction of the North Lancangjiang Paleo-Tethyan slab under the North Qiangtang block, and the second stage represents the collision between the North and South Qiangtang blocks (Fig. 8). This evolution of the Paleo-Tethyan system is similar to that proposed in the central Qiangtang area to the west (Zhai et al., 2016), the Simao area (Wu et al., 1995; Peng et al., 2008), and Thailand to the southeast (Gardiner et al., 2016). Limited research in the Qamdo area means that the Jinhong–Nan River backarc of southeastern Asia (Peng et al., 2008; Sone and Metcalfe, 2008; Metcalfe, 2013) has not been identified in this area to date. This means that further research is needed to determine whether a backarc basin existed in the Qamdo area between the Late Permian and Middle Triassic.

Closure of the Jinshajiang Paleo-Tethys Ocean

The Jinshajiang suture crops out in eastern Tibet and separates the Qamdo area from the Songpan-Ganzi flysch belt and the South China block (Fig. 1). Biostratigraphic data constrain the age of an ophiolite in this region to early Carboniferous–Permian (Sun et al., 1997). Zircon U-Pb ages of 340 ± 3 Ma and 294 ± 3 Ma for plagiogranites within this ophiolite indicate that the Jinshajiang oceanic lithosphere formed during the early Carboniferous (Wang et al., 2000). In addition, a cumulate gabbro-anorthosite association and an amphibole gabbro yielded ages of 338 ± 6 Ma and 320 ± 10 Ma (Jian et al., 2009), respectively, thereby further constraining the timing of formation of the Jinshajiang oceanic crust. The fact that the oceanic basin stage of the Jinshajiang belt is too short to separate the Gondwanan biogeographic provinces from the Cathaysian biogeographic provinces means that the Jinshajiang suture zone represents only a branch-type structure in the Paleo-Tethys region.

Permian–Triassic granites are observed mainly to the west of the Jinshajiang ophiolite mélange zone (BGMRX, 1993), indicating that the Songpan-Ganzi flysch belt was thrust westward under the North Qiangtang block during the closure of the Paleo-Tethys Ocean. Geochronological and geochemical data from the Baimaxueshan pluton of the Deqin area to the south of the study area and granite plutons from the Yushu area to the north of the study area indicate that the 275–248 Ma granites in this area are arc-like granites. These dates therefore indicate the timing of the westward subduction stage of the Jinshajiang Paleo-Tethyan slab beneath the Qamdo block (Yang et al., 2011; Zi et al., 2012). The geochemistry of the 233.5–229.6 Ma Batang granites is indicative of formation in a syncollisional environment representing the second stage of convergence between the Qamdo and South China blocks. This model is supported by geochronological and geochemical data from granites to the south of the study area (Wang et al., 2000), but the timing of this collision between the North Qiangtang block and the Songpan-Ganzi flysch belt was much earlier than the 200 Ma final formation age of the Songpan-Ganzi flysch (Zhang et al., 2012). However, this contrast in timing can be explained by the presence of a remnant sea after the collision of these blocks. In addition, the Paleo-Tethyan evolution inferred from the intrusion of granite plutons into the Jinshajiang ophiolite mélange is consistent with geochronological data from HP-UHP belts and ophiolitic mélanges between central Tibet and southeastern Asia (e.g., Wu et al., 1995; Jian et al., 2009; Yang et al., 2011). Combining the results of previous research with the data presented in the present study allows the evolution of the Jinshajiang Paleo-Tethys to be divided into subduction (275–248 Ma) and collision (232–229 Ma) stages (Fig. 8) that are similar to the evolution of the Song Ma suture (Metcalfe, 2013; Wang et al., 2016). Therefore, our results show that over a distance of ~4000 km, from the central Qiangtang area to the Indochina region, the evolution of the Jinshajiang Paleo-Tethyan system is consistent, which implies an affinity among the

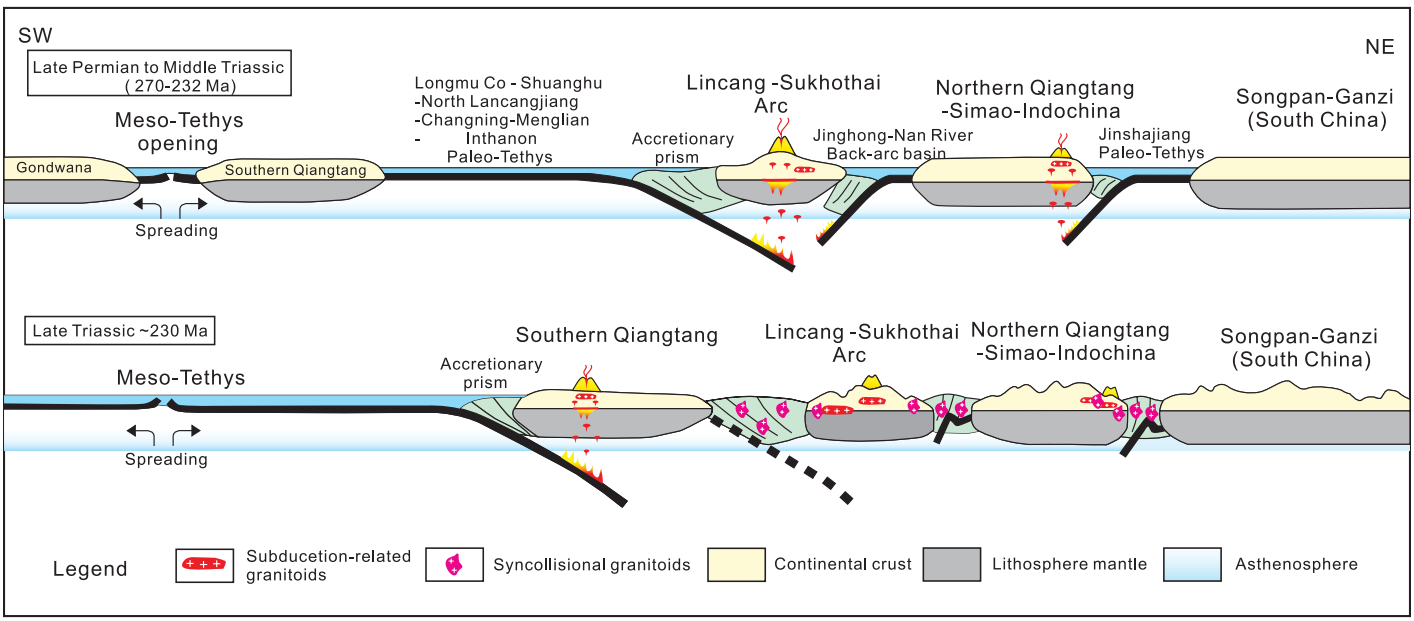

Figure 8. Geodynamic model of convergence among the North Qiangtang block and surrounding blocks during closure of the Paleo-Tethys Ocean (after Peng et al., 2008, 2015; Jian et al., 2009; Tao et al., 2014).

North Qiangtang, Simao, and Indochina blocks, as previously inferred (Metcalfe, 2013; Wang et al., 2016).

Single North Qiangtang–Simao–Indochina Block

Our samples from the North Qiangtang block yielded peaks in Hf and Nd T_{DM2} ages at ca. 2.0–1.6 and 1.2–0.8 Ga, consistent with those acquired from the Simao and Indochina regions (Lan et al., 2003; Wang et al., 2014, 2016). This correspondence indicates that in both the Qamdo region and southeastern Asia, the basement formed during the middle Mesoproterozoic–early Paleozoic. North Qiangtang and Indochina Paleozoic strata contain similar warm-climate fossils (Sone and Metcalfe, 2008; Metcalfe, 2013), indicating that these regions were connected during the early Paleozoic. In contrast, the South Qiangtang block consists of pan-African basement overlain by early Paleozoic cover sequences containing Gondwanan cold-water fauna, similar to the Baoshan-Sibumasu block, which represents an eastern segment of the Cimmerian block (Li et al., 2009; Metcalfe, 2013). Furthermore, the Inthanon, Changning-Menglian, Longmu Co–Shuanghu, and Song Ma–Jinshajiang suture zones that bound the North Qiangtang, Simao, and Indochina blocks are continuous, and the timing and style of block convergence are similar from North Qiangtang to southeastern Asia. In addition, there is no evidence of a suture zone between the Qamdo, Simao, and Indochina microcontinents. All the above evidence supports the proposal that North Qiangtang, Simao, and Indochina represent a single block (e.g., Sone and Metcalfe, 2008; Metcalfe, 2013; Wang et al., 2016, 2018).

The Turkey, Iran, South Qiangtang, Baoshan, and Sibumasu blocks constituted the 7000-km-long Cimmerian block that existed during the opening of the Paleo-Tethys Ocean (Şengör, 1984; Metcalfe, 2013). The evolution of the Paleo-Tethys recorded in the North Qiangtang and Indochina blocks (e.g., Zhai et al., 2016; Metcalfe, 2013; Wang et al., 2016, 2018) and the data presented in the present study suggest that the North Qiangtang, Simao, and Indochina blocks constituted a 3000–4000-km-long block that was parallel to the Cimmerian block at this time (Fig. 9).

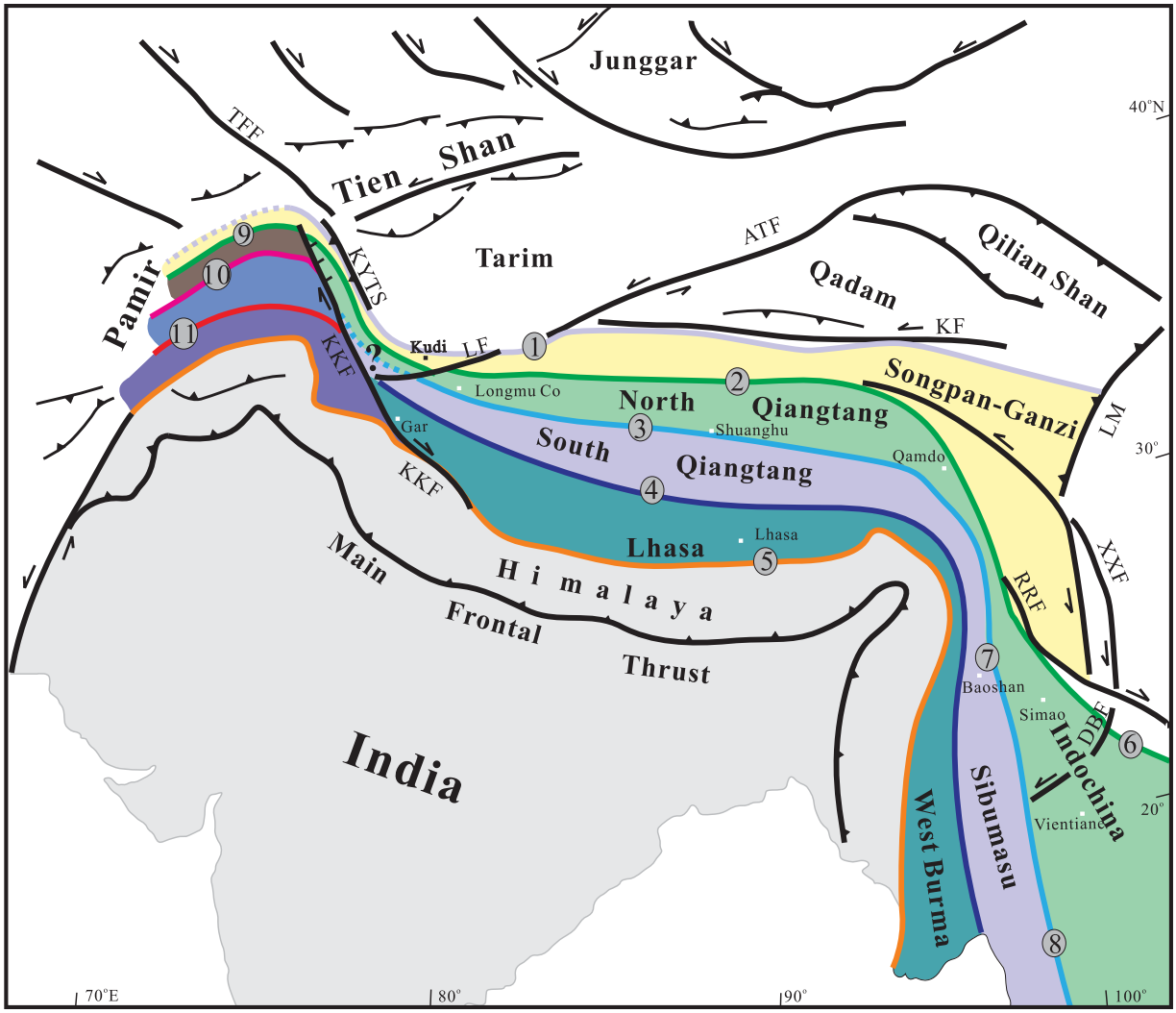

Figure 9. Preliminary correlation of tectonic blocks in the Tibetan Plateau and southeastern Asia. 1—Kudi suture; 2—Jinshajiang suture; 3—Longmu Co–Shuanghu suture; 4—Bangong Co–Nujiang suture; 5—Yalong–Zangpo suture; 6—Song Ma suture; 7—Changning–Menglian suture; 8—Inthanon suture; 9—Tanymas suture; 10—Rushan–Pshart suture; 11—Shyok suture. Abbreviations are as follows: TFF—Talas–Fergana fault; ATF—Altyn Tagh fault; KKF—Karakorum fault; LF—Longmu Co fault; KF—East Kunlun fault; LM—Longmen thrust fault; XXF—Xianshuihe-Xiaojiang fault; DBF—Dien Bien Phu fault; KYTS—Kashgar-Yecheng-Tiklik fault system; RRF—Red River fault.

CONCLUSIONS

New zircon LA-ICP-MS U-Pb ages indicate that the granitic Chaya and Jinba plutons of the NLMB were emplaced at ca. 267 and ca. 233 Ma, respectively, whereas the granitic Batang pluton within the Jinshajiang suture zone was emplaced around 230 Ma. The geochemistry of the Chaya pluton indicates that these I-type arc-related magmatic rocks of the Chaya pluton record upper-mantle and subduction processes during the emplacement of the pluton. In contrast, the peraluminous S-type Jinba granites were sourced from metapelites that interacted with mantle-derived juvenile crust during collision between the North and South Qiangtang blocks. The geochemistry of the syncollisional Batang granites also indicates that this pluton formed from magmas derived from a metabasaltic source within the lower crust.

The inferred origins of the studied plutons support the hypothesis that convergence among the North Qiangtang and adjacent blocks occurred during the closure of the Paleo-Tethys Ocean. During this process, the North Lancangjiang Paleo-Tethyan slab subducted beneath the North Qiangtang block to the west, and the Yangtze block was thrust under the North Qiangtang block to the east. Hf and Nd T_{DM2} model ages from the studied plutons indicate a Columbia-Rodinia affinity, similar to Simao and Indochina basement. In summary, data from the basement and cover sequences of the North Qiangtang, Simao, and Indochina blocks and their shared Paleo-Tethys history all suggest that these blocks represent a single block that was located parallel to the Cimmerian block during the Early Permian to Early Triassic (or before 230 Ma).

ACKNOWLEDGMENTS

This study was financially supported by the National Key R&D Program of China (2018YFC1505001) and the China Geological Survey (project 121201101000150014). We thank Li Zhengyou, Wang Xinyu, and Duan Lei for their assistance during field work as well as several anonymous reviewers for comments that helped to improve the original manuscript.

REFERENCES CITED

Andersen, T., 2002, Correction of common Pb in U-Pb analyses that do not report ^{204}Pb: Chemical Geology, v. 192, p. 59–79, https://doi.org/10.1016/S0009-2541(02)00195-X.

Angiolini, L., Zanchi, A., Zanchetta, S., Nicora, A., and Vezzoli, G., 2013, The Cimmerian geopuzzle: New data from South Pamir: Terra Nova, v. 25, p. 352–360, https://doi.org/10.1111/ter.12042.

Blichert-Toft, J., and Albarede, F., 1997, The Lu-Hf geochemistry of chondrites and the evolution of the mantle-crust system: Earth and Planetary Science Letters, v. 148, p. 243–258, https://doi.org/10.1016/S0012-821X(97)00040-X.

Boynton, W.V., 1984, Cosmochemistry of the rare earth elements: Meteorite studies, *in* Henderson, P., ed., Rare Earth Element Geochemistry: Amsterdam, Netherlands, Elsevier, p. 63–114, https://doi.org/10.1016/B978-0-444-42148-7.50008-3.

Bureau of Geology and Mineral Resources of Xizang Province (BGMRX), 1993, Regional Geology of Xizang Province: Beijing, Geological Publishing House [in Chinese].

Chappell, B.W., and White, A.J.R., 1992, I- and S-type granites in the Lanchlan fold belt: Transactions of the Royal Society of Edinburgh–Earth Sciences, v. 83, p. 1–26, https://doi.org/10.1017/S0263593300007720.

Chen, F.K., Li, X.H., Wang, X.L., Li, Q.L., and Siebel, W., 2007, Zircon age and Nd-Hf isotopic composition of the Yunnan Tethyan belt, southwestern China: International Journal of Earth Sciences, v. 96, no. 6, p. 1179–1194, https://doi.org/10.1007/s00531-006-0146-y.

Clemens, J.D., 2003, S-type granitic magmas—Petrogenetic issues, models and evidence: Earth-Science Reviews, v. 61, p. 1–18, https://doi.org/10.1016/S0012-8252(02)00107-1.

Gardiner, N.J., Searle, M.P., Morley, C.K., Whitehouse, M.P., Spencer, C.J., and Robb, L.J., 2016, The closure of Palaeo-Tethys in eastern Myanmar and northern Thailand: New insights from zircon U-Pb and Hf isotope data: Gondwana Research, v. 39, p. 401–422, https://doi.org/10.1016/j.gr.2015.03.001.

Gertisser, R., and Keller, J., 2003, Trace element and Sr, Nd, Pb and O isotope variations in medium-K and high-K volcanic rocks from Merapi volcano, central Java, Indonesia: Evidence for the involvement of subducted sediments in Sunda arc magma genesis: Journal of Petrology, v. 44, p. 457–489, https://doi.org/10.1093/petrology/44.3.457.

Griffin, W.L., Pearson, N.J., Belousova, E., Jackson, S.E., van Achterbergh, E., O'Reilly, S.Y., and Shee, S.R., 2000, The Hf isotope composition of cratonic mantle: LA-MC-ICP-MS analysis of zircon megacrysts in kimberlites: Geochimica et Cosmochimica Acta, v. 64, p. 133–147, https://doi.org/10.1016/S0016-7037(99)00343-9.

Jian, P., Liu, D.Y., Kröner, A., Zhang, Q., Wang, Y.Z., Sun, X.M., and Zhang, W., 2009, Devonian to Permian plate tectonic cycle of the Paleo-Tethys orogen in southwest China (I): Geochemistry of ophiolites, arc/back-arc assemblages and within-plate igneous rocks: Lithos, v. 113, p. 748–766, https://doi.org/10.1016/j.lithos.2009.04.004.

Jung, S., and Pfänder, J.A., 2007, Source composition and melting temperatures of orogenic granitoids: constraints from CaO/Na_2O, Al_2O_3/TiO_2 and accessory mineral saturation thermometry: European Journal of Mineralogy, v.19, p.859–870.

Lan, C.-Y., Chung, S.-L., Long, T.V., Lo, C.-H., Lee, T.-Y., Mertzman, S.A., and Shen, J.J.-S., 2003, Geochemical and Sr -Nd isotopic constraints from the Kontum massif, central Vietnam, on the crustal evolution of the Indochina block: Precambrian Research, v. 122, p. 7–27, https://doi.org/10.1016/S0301-9268(02)00205-X.

Li, C., Zhai, Q.G., Dong, Y.S., Liu, S., Xie, C.M., and Wu, Y.W., 2009, High-pressure eclogite-blueschist metamorphic belt and closure of paleo-Tethys Ocean in central Qiangtang, Qinghai–Tibet Plateau: Journal of Earth Science, v. 20, p. 209–218, https://doi.org/10.1007/s12583-009-0021-4.

Liu, Y.S., Hu, Z.C., Gao, S., Günther, D., Xu, J., Gao, C.G., and Chen, H.H., 2008, In situ analysis of major and trace elements of anhydrous minerals by LA-ICP-MS without applying an internal standard: Chemical Geology, v. 257, p. 34–43, https://doi.org/10.1016/j.chemgeo.2008.08.004.

Ludwig, K. R., 2003, Users' Manual for Isoplot/Ex Rev. 3.0: Berkeley Geochronology Center Special Publication 1a, 55 p.

Maniar, P.D., and Piccoli, P.M., 1989, Tectonic discrimination of granitoids: Geological Society of America Bulletin, v. 101, p. 635–643, https://doi.org/10.1130/0016-7606(1989)101<0635:TDOG>2.3.CO;2.

Metcalfe, I., 2013, Gondwana dispersion and Asian accretion: Tectonic and palaeogeographic evolution of the eastern Tethys: Journal of Asian Earth Sciences, v. 66, p. 1–33, https://doi.org/10.1016/j.jseaes.2012.12.020.

Middlemost, E.A.K., 1994, Naming materials in the magma/igneous rock system: Earth-Science Reviews, v. 37, p. 215–224, https://doi.org/10.1016/0012-8252(94)90029-9.

Miller, C.F., Mcdowell, S.M., and Mapes, R.W., 2003, Hot and cold granites? Implications of zircon saturation temperatures and preservation of inheritance: Geology, v. 31, no. 6, p. 529–532, https://doi.org/10.1130/0091-7613(2003)031<0529:HACGIO>2.0.CO;2.

Murphy, J.B., Shellnutt, J.G., and Collins, W.J., 2018, Late Neoproterozoic to Carboniferous genesis of A-type magmas in Avalonia of northern Nova Scotia: Repeated partial melting of anhydrous lower crust in contrasting tectonic environments: International Journal of Earth Sciences, v. 107, p. 587–599, https://doi.org/10.1007/s00531-017-1512-7.

Pan, G., Wang, L., Li, R., Yin, F., and Zhu, D., 2012, Tectonic model of archipelagic arc–basin systems: The key to the continental geology: Sedimentary Geology and Tethyan Geology, v. 32, no. 3, p. 516 [in Chinese with English abstract].

Patiño Douce, A.E., 1999, What do experiments tell us about the relative contributions of crust and mantle to the origin of granitic magmas?, *in* Castro, A., Fernandez, C., and Vigneresse, J.L., eds., Understanding Granites: Integrating New and Classical Techniques: Geological Society, London, Special Publication 168, p. 55–75.

Pearce, J.A., and Peate, D.W., 1995, Tectonic implications of the composition of volcanic arc magmas: Annual Review of Earth and Planetary Sciences, v. 23, p. 251–285, https://doi.org/10.1146/annurev.ea.23.050195.001343.

Peccerillo, A., and Taylor, S.R., 1976, Geochemistry of Eocene calc-alkaline volcanic rocks from the Kastamonu area, northern Turkey: Contributions to Mineralogy and Petrology, v. 58, p. 63–81, https://doi.org/10.1007/BF00384745.

Peng, T., Wang, Y., Zhao, G., Fan, W., and Peng, B., 2008, Arc-like volcanic rocks from the southern Lancangjiang zone, SW China: Geochronological and geochemical constraints on their petrogenesis and tectonic implications: Lithos, v. 102, p. 358–373, https://doi.org/10.1016/j.lithos.2007.08.012.

Peng, T., Zhao, G., Fan, W., Peng, B., and Mao, Y., 2015, Late Triassic granitic magmatism in the eastern Qiangtang, eastern Tibetan Plateau: Geochronology, petrogenesis and implications for the tectonic evolution of the Paleo-Tethys: Gondwana Research, v. 27, no. 4, p. 1494–1508, https://doi.org/10.1016/j.gr.2014.01.009.

Petford, N., and Atherton, M., 1996, Na-rich partial melts from newly underplated basaltic crust: The Cordillera Blanca Batholith, Peru: Journal of Petrology, v. 37, p. 1491–1521, https://doi.org/10.1093/petrology/37.6.1491.

Rapp, R.P., Watson, E.B., and Miller, C.F., 1991, Partial melting of amphibolite/eclogite and the origin of Archean trondhjemites and tonalites: Precambrian Research, v. 51, no. 1–4, p. 1–25, https://doi.org/10.1016/0301-9268(91)90092-O.

Royden, H.L., Burchfiel, B.C., and van der Hilst, D.R., 2008, The geological evolution of the Tibetan Plateau: Science, v. 321, p. 1054–1058, https://doi.org/10.1126/science.1155371.

Schwab, M., Ratschbacher, L., Siebel, W., McWilliams, M., Minaev, V., Lutkov, V., Chen, F., Stanek, K., Nelson, B., Frisch, W., and Wooden, J.L., 2004, Assembly of the Pamirs: Age and origin of magmatic belts from the southern Tien Shan to the southern Pamirs and their relation to Tibet: Tectonics, v. 23, TC4002, https://doi.org/10.1029/2003TC001583.

Şengör, A.M.C., 1984, The Cimmeride Orogenic System and the Tectonics of Eurasia: Geological Society of America Special Paper 195, 182 p.

Sone, M., and Metcalfe, I., 2008, Parallel Tethyan suture in mainland Southeast Asia: New insights from Paleo-Tethys closure and implications for the Indosinian orogeny: Comptes Rendus Geoscience, v. 340, p. 166–179, https://doi.org/10.1016/j.crte.2007.09.008.

Sun, S., and McDonough, W.F., 1989, Chemical and isotopic systematics of oceanic basalts: Implications for mantle composition and processes, *in* Saunders, A.D., and Norry, M.J., eds., Magmatism in the Ocean Basins: Geological Society, London, Special Publication 42, p. 313–345, https://doi.org/10.1144/GSL.SP.1989.042.01.19.

Sun, X., Zhang, B., Nie, Z., and Liang, D., 1997, Formation age and environment of ophiolite and ophiolitic mélange in the Jinshajiang belt, northwest Yunnan: Dizhi Lunping, v. 43, p. 113–120.

Tao, Y., Bi, X., Li, C., Hu, R., Li, Y., and Liao, M., 2014, Geochronology, petrogenesis and tectonic significance of the Jitang granitic pluton in eastern Tibet, SW China: Lithos, v. 184–187, p. 314–323, https://doi.org/10.1016/j.lithos.2013.10.031.

Vuong, N.V., Hansen, B.T., Wemmer, K., Lepvrier, C., Vu Van Tich, and Ta Trong Thang, 2013, U/Pb and Sm/Nd dating on ophiolitic rocks of the Song Ma suture zone (northern Vietnam):

Evidence for Upper Paleozoic Paleotethyan lithospheric remnants: Journal of Geodynamics, v. 69, no. 3, p. 140–147.

Wang, L., Liu, C., Gao, X., and Zhang, H., 2014, Provenance and paleogeography of the Late Cretaceous Mengyejing Formation, Simao Basin, southeastern Tibetan Plateau: Whole-rock geochemistry, U-Pb geochronology, and Hf isotopic constraints: Sedimentary Geology, v. 304, p. 44–58, https://doi.org/10.1016/j.sedgeo.2014.02.003.

Wang, S., Mo, Y., Wang, C., and Ye, P., 2016, Paleotethyan evolution of the Indochina block as deduced from granites in northern Laos: Gondwana Research, v. 38, p. 183–196, https://doi.org/10.1016/j.gr.2015.11.011.

Wang, X., Metcalfe, I., Jian, P., He, L., and Wang, C., 2000, The Jinshajiang-Ailaoshan suture zone: Tectono-stratigraphy, age and evolution: Journal of Asian Earth Sciences, v. 18, p. 675–690, https://doi.org/10.1016/S1367-9120(00)00039-0.

Wang, X., Wang, S., Wang, C., and Chen, L., 2018, Late Permian to Late Triassic arc-like granitoids in the northern Lancangjiang tectonic belt, eastern Tibet: Age, geochemistry, Sr-Nd-Hf isotopes and tectonic implications: Lithos, v. 308–309, p. 278–293, https://doi.org/10.1016/j.lithos.2018.03.008.

Watson, E.B., and Harrison, T.M., 1983, Zircon saturation revisited: Temperature and composition effects in a variety of crustal magma types: Earth and Planetary Science Letters, v. 64, p. 295–304, https://doi.org/10.1016/0012-821X(83)90211-X.

Wu, F., Li, X., Zheng, Y., and Gao, S., 2007, Lu-Hf isotopic systematics and their applications in petrology: Acta Petrologica Sinica (Yanshi Xuebao), v. 23, no. 2, p. 185–220 [in Chinese with English abstract].

Wu, H., Boulter, C.A., Ke, B., Stow, D.A.V., and Wang, Z., 1995, The Changning-Menglian suture zone; a segment of the major Cathaysian-Gondwana divide in Southeast Asia: Tectonophysics, v. 242, p. 267–280, https://doi.org/10.1016/0040-1951(94)00210-Z.

Xie, J., Li, W., Dong, G., Mo, X., Zhao, Z., Yu, J., and Wang, T., 2013, Petrology, geochemistry and tectonic significance of the granites from Basu area, Tibet: Acta Petrologica Sinica, v. 29, p. 3779–3791.

Xu, Y., He, B., Chung, S.L., Menzies, M., and Frey, F.A., 2004, Geologic, geochemical, and geophysical consequences of plume involvement in the Emeishan flood-basalt province: Geology, v. 32, p. 917–920, https://doi.org/10.1130/G20602.1.

Yang, T., Zhang, Y., Liu, Y., Wang, Z., Song, Y., Yang, Z., and Tian, S., 2011, 2011, Permo-Triassic arc magmatism in central Tibet: Evidence from zircon U-Pb geochronology, Hf isotopes, rare earth elements, and bulk geochemistry: Chemical Geology, v. 284, p. 270–282, https://doi.org/10.1016/j.chemgeo.2011.03.006.

Zhai, Q., Jahn, B., Wang, J., Hu, P., Chung, S., Lee, H., and Tang, S., 2016, Oldest Paleo-Tethyan ophiolitic mélange in the Tibetan Plateau: Geological Society of America Bulletin, v. 128, no. 3/4, p. 355–373, https://doi.org/10.1130/B31296.1.

Zhang, K., Cai, J., Zhang, Y., and Zhao, T., 2006, Eclogites from central Qiangtang, northern Tibet (China), and tectonic implications: Earth and Planetary Science Letters, v. 245, p. 722–729, https://doi.org/10.1016/j.epsl.2006.02.025.

Zhang, K., Li, B., and Wei, Q., 2012, Geochemistry and Nd isotopes of the Songpan-Ganzi Triassic turbidites, central China: Diversified provenances and tectonic implications: The Journal of Geology, v. 120, p. 69–82, https://doi.org/10.1086/662716.

Zhu, J., Hu, R., Bi, X., Zhong, H., and Chen, H., 2013, Zircon U-Pb ages, Hf-O isotopes and whole-rock Sr-Nd-Pb isotopic geochemistry of granitoids in the Jinshajiang suture zone, SW China: Constraints on petrogenesis and tectonic evolution of the Paleo-Tethys Ocean: Lithos, v.126, p.248–264.

Zi, J., Cawood, P.A., Fan, W., Wang, Y., Tohver, E., McCuaig, T., and Peng, T., 2012, Triassic collision in the Paleo-Tethys Ocean constrained by volcanic activity in SW China: Lithos, v. 144–145, p. 145–160, https://doi.org/10.1016/j.lithos.2012.04.020.

MANUSCRIPT RECEIVED 19 JUNE 2018
REVISED MANUSCRIPT RECEIVED 9 JANUARY 2019
MANUSCRIPT ACCEPTED 29 JANUARY 2019